Check for updates

Recent changes in the rain regime over the Mediterranean climate region of Israel

Ron Drori[1] · Baruch Ziv[1,2] · Hadas Saaroni[3] · Adi Etkin[3] · Efrat Sheffer[1]

Abstract

Previous observational analyses have shown a declining rainfall trend over Israel, mostly statistically insignificant. The current study, for the period 1975–2020, undermines these findings, and the alarming future projections, and elaborates other ingredients of the rain regime. No trend is found for the annual rainfall, reflecting a balance between a negative trend in the number of rainy days and a positive trend in the daily rainfall intensity, both on the order of 2.0%/decade. In the mid-winter, the rainfall and the daily intensity increased, while both declined in the autumn and spring, implying a contraction of the rainy season. The time span between accumulation of 10% and 90% of the annual rainfall, being 112 days on the average, shortened by 7 days during the study period. This is also expressed by an increase of the Seasonality Index, indicating that the regional climate is shifting from "markedly seasonal with a long dry season" to "most rain in ≤3 months." The intra-seasonal course of the rainfall trend corresponds to that of the occurrence and intensity of the Cyprus Lows and the Mediterranean Oscillation. The contraction of the rainy season and the increase in the daily intensity have far-reaching environmental impacts in this vulnerable region.

✉ Hadas Saaroni
  saaroni@tauex.tau.ac.il

1   The Robert H. Smith Institute of Plant Sciences and Genetics in Agriculture, The Hebrew University of Jerusalem, Jerusalem, Israel

2   Department of Natural Sciences, The Open University of Israel, Ra'anana, Israel

3   The Porter School of the Environment and Earth Sciences, Tel-Aviv University, Tel-Aviv, Israel

1 Introduction

The East Mediterranean (EM) is located on a sharp climatic gradient between Mediterranean climate in its northern part and arid climate in its south. This region is vulnerable to precipitation variations (e.g., Lionello and Giorgi 2007; Giorgi and Lionello 2008), since any change in the rain regime may result in a shift of the climatic borders between the Mediterranean, semi-arid, and arid climates, which is crucial for water availability to biological and ecological processes. For example, a recent study (Kelley et al. 2015) linked the Syrian uprising before 2011 with the unusually long drought in the greater Fertile Crescent. Plants growing in arid and Mediterranean climate regions are adapted to low rainfall availability and strong seasonality (Blondel et al. 2010). However, such drought-adapted vegetation may not be resilient to further reduction in rainfall or elongation of the summer dry period (Schlaepfer et al. 2017; Winkler et al. 2019). Another risk associated with global warming is exacerbation of fires on the one hand, and of flooding due to increase in the rainfall intensity on the other hand (Hoegh-Guldberg et al. 2018).

Cyprus Lows (CLs), which are mid-latitude cyclones (Alpert et al. 1990; Ulbrich et al. 2012), are the major rain contributors in Israel, and are responsible for 90% of the annual rainfall (Goldreich et al. 2004). A significant correlation was found between the number of CL days and the annual rainfall in the Mediterranean and semi-arid climate regions of Israel (Saaroni et al. 2010). The CLs prevail in the winter and the transitional seasons and are absent in the summer. Accordingly, the rainy season is confined to the months October–May, whereas two-third of the annual rainfall is obtained in the mid-winter months, December–February (DJF, Goldreich 2003).

While a CL exists in the EM, cold air originating from Europe moves over the warm Mediterranean water and becomes unstable before entering Israel. The Mediterranean Sea is regarded as the moisture contributor for the rains that are associated with CLs (Shay-El and Alpert 1991; Saaroni et al. 2010). A significant correlation was found between the heat storage in the upper layers of the southeast Mediterranean and winter precipitation in Israel by Tzvetkov and Assaf (1982), who also found a higher correlation between the seasonal heat storage depletion from the EM during the rainy season and the rainfall. They approximated the heat storage depletion by $\rho C_p D \, \Delta T$, where ρ is the water density, C_p is specific heat of the water, D is the depth of the upper layer (138 m deep), and ΔT is the sea temperature depletion during the rainy season. This is attributed to the increase in evaporation rate with temperature, implied by the Clausius–Clapeyron relation. A synoptic classification for the EM (Alpert et al. 2004a) differentiates among seven types of CLs, according to their location with respect to Israel and their intensity (dividing them to "deep" and "shallow" CLs); three of them are exemplified in Fig. 1. A minor portion of the rainfall in Israel is contributed by penetrations of warm and humid air masses, originating from the tropics. These are active Red Sea troughs and tropical plumes (e.g., Ziv 2001; Alpert et al. 2005; Rubin et al. 2007; Shalev et al. 2011; De Vries et al. 2013; Krichak et al. 2015).

Most of the observational evidence over the latest decades indicate a drying trend in the Mediterranean region (e.g., Xoplaki et al. 2004; Kostopoulou and Jones 2005; Toreti et al. 2010; Hoegh-Guldberg et al. 2018). Raymond et al. (2018), in their analysis of very long dry spells over the Mediterranean (longer than the 80th percentile of dry spells), found a general increasing trend, though did not report on any significant results. The drying trend over the EM has been attributed, among others, to the expansion of the Hadley cell poleward due to the global warming (Lu et al. 2007; Previdi and Liepert 2007; Seidel et al. 2008; Johanson and Fu
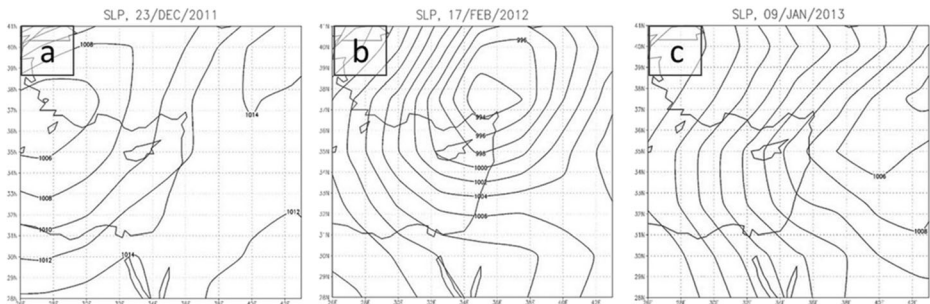
Fig. 1 Sea-level pressure (SLP, hPa) maps exemplifying three of the CL types, defined by Alpert et al. (2004a): **a** CL west of Cyprus, **b** deep CL north of Israel, and **c** deep CL east of Israel

2009; Seager et al. 2010). Since the Mediterranean is located during the winter and the transitional seasons north of the descending branch of the Hadley cell, its northward expansion is expected to suppress the cyclonic activity over that region, resulting in rainfall reduction.

As for the rainfall intensity, a global general increase is expected (IPCC 2018). An analysis of trends in the distribution of daily rainfall was done for the Mediterranean region for the period 1951–1995 (Alpert et al. 2002). It indicated a 4-fold increase in torrential rainfall, exceeding 128 mm/day, in Italy and a similar increase in heavy torrential rain (> 64 mm/day) in Spain.

In Israel, drying trends have been found for the recent decades, mostly statistically insignificant (Alpert et al. 2002; Yosef et al. 2009; Shohami et al. 2011; Ziv et al. 2014; Yosef et al. 2019). A significant drying trend in the spring months (March–May) was found by Ziv et al. (2014) for 1975–2010. They also showed a decrease in the number of rainy days and a retrograding trend in the time by which 90% of the annual rainfall is accumulated, denoting the end of the rainy season, at a rate of 3 days/decade. For the period 1950–2017, a reduction in the annual rainfall and in the number of wet days was found by Yosef et al. (2019). Though the individual and regional trends were not statistically significant, they showed a fine spatial coherence. For the latest 30 years, 1988–2017, they found similar results, but with higher decline trend for both rainfall and the number of wet days, though still statistically insignificant. The masking effect of large natural variance in precipitation was elaborated by Morin (2011). The author shows that for a 40-year record, the change in the annual rainfall must be at least as large as the standard deviation in order to be detected with a probability of more than 50%.

The distribution of daily rainfall in Israel did not show significant trends during the period 1951–1995 (Alpert et al. 2002). For the period 1951–2004, an increase in the relative contribution of days with >32 mm was found at the center and southern parts of Israel and a decrease in the north, though statistically insignificant (Yosef et al. 2009). A tendency toward more intense wet days was found by Yosef et al. (2019) for the period 1950–2017, with higher rates for the period 1988–2017 (both statistically insignificant). Based on the ratio between the relative decrease in the number of rainy days with respect to the decrease in the total rainfall, Ziv et al. (2014) deduced that for the period 1975–2010, the average daily rainfall increased.

Several studies examined trends in factors that may explain rainfall trends in Israel, the occurrence of CLs, the magnitude of large-scale oscillations, and the lower-level moisture availability. The trend of CLs' occurrence for the period 1948–2000 was analyzed by Alpert et al. (2004a), who did not find any consistent trend. For the period 1965–2003, a significant

reduction in cyclogenesis, defined by the occurrence of CLs according to the classification of Alpert et al. (2004a), was shown by Shohami et al. (2011). As for large-scale oscillations, Alpert et al. (2004a) indicated rainfall oscillations in the timescale of 20 years, which they attributed to the North Atlantic Oscillation (NAO). Nevertheless, the correlation between the NAO and the rainfall in Israel, on the annual scale, was examined by Ziv et al. (2006) and Ziv et al. (2014) and found negligible. The Mediterranean Oscillation Index (MOI2), defined as the upper-level pressure difference between the western and eastern parts of the Mediterranean (Palutikof 2003), was found significantly correlated with the rainfall in Israel (Ziv et al. 2014). Higher MOI2 reflects an intensification of the Azores High and/or enhancement of the cyclonic activity over the EM and vice versa. Accordingly, this index is a manifestation of the seesaw relation in the cyclonic activity between the eastern and western Mediterranean (e.g., Raible et al. 2010). The 700-hPa specific humidity was shown to significantly decrease over the EM during the winters and the transitional seasons for the rainy seasons 1965–2003 (Shohami et al. 2011). They suggested that this reduction, together with the decrease in cyclogenesis, explain the reduction in rainfall they found.

Future projections for the EM indicate a consistent declining trend of the annual rainfall and of the occurrence of CLs. Considerable precipitation decreases over the EM and North Israel were predicted by Alpert et al. (2008), based on regional climate models. A decrease of about 10% in the mean annual precipitation over the EM by the end of the twenty-first century was projected by Chenoweth et al. (2011) and Lelieveld et al. (2012), based on the PRECIS model. A decrease of 20–35% in total precipitation and in the number of wet days over the EM at the end of the twenty-first century was projected by Samuels et al. (2017), based on CMIP5 models (RCP8.5 scenario).

Regarding expected changes in CLs' occurrence, a 35% reduction toward the end of the twenty-first century was projected by Hochman et al. (2018a), based on CMIP5 models (RCP8.5 scenario). Following this projection, the duration of the winter season (as defined by Alpert et al. 2004b) was shown by Hochman et al. (2018b) to shorten by 25% in the mid-century (2046–2065) and by 56% at the end of the twenty-first century (2081–2100). Using high-resolution (~8 km) climate projections for Israel, based on COSMO-CLM, nested into the CORDEX-MENA simulations (at 25 km resolution), Hochman et al. (2018c) projected a precipitation decrease in the Mediterranean climate region of Israel, reaching ~40% in 2041–2070, according RCP4.5. In contrast to the expected rainfall decrease, they projected an increase in rain intensity, mostly for the southern, arid part of the region, with some indications of extremity also in the north of Israel. A most recent study (Takeshima et al. 2020) projects a significant and intense drying over several regions of the world, including the Mediterranean, indicated by all four models applied for both the 1.5° and 2.0 °C warming. They project that extreme dry-years will become 2–3 times more likely over the Mediterranean.

The severe drying in Israel implied by the future projections has been supported by observational evidence. However, the trends identified are based on different study periods and show insignificant results. According to the IPCC (2018), the period of persistent global warming starts from the mid-1970s. The only study addressing the regional rainfall trend during this period (Ziv et al. 2014) ends in 2010. In light of the considerable drying trend projected for this region and the large fluctuations during the latest decade (2011–2020), it is essential to re-examine the trends in the components of the rain regime and its controlling factors up to 2020. It should be noted that this latest decade is challenging for assessing the drying trend, since it included several extreme rainy seasons such as the driest season in North Israel (2013/14, denoted as 2014) and the two consecutive wet seasons, with over 130% of the

annual mean (2019 and 2020), according to the reports of the Israeli Meteorological Service (IMS). Besides the need to extend the trend analysis up to 2020, this study intends to bridge the knowledge gap of the combined impact of the synoptic and thermodynamic factors governing the rain regime over Israel.

The objective of the current study is to analyze trends in the rain regime of Israel for 1975–2020, including:

- The rainfall, the number of rainy days, and the daily rainfall intensity on the annual and the intra-seasonal (SON, DJF, MAM) timescales.
- The length of the rainy season and the concentration of the rain with respect to the center of the season, based on the Seasonality Index (*SI*) of Walsh and Lawler (1981).
- The contribution of the governing factors: the occurrence and intensity of the CLs, the MOI2, the specific humidity, and the sea surface temperature (SST) over the EM, through multi-linear regression.

2 Materials

2.1 Data

The study refers to the following rain variables: annual rainfall, daily average rainfall intensity (both are based on all the rainy days, with >0.1 mm), and the number of rainy days (days with ≥1.0 mm). The threshold for defining a rainy day is according to the definition of effective rainy day by the IMS (Yosef et al. 2019). The contribution of days with <1 mm to the total rainfall was found to be less than 1.8%. The daily rain data were taken from the IMS network (https://ims.data.gov.il/he/ims/3). We used 51 rain stations located north of 31°20′N (annual average rainfall >200 mm, see Fig. 1), which have recently been homogenized by the IMS (Yosef et al. 2019). The term "annual" refers to the "rainy season," which lasts between October and May and officially starts on 1 August and ends on 31 July. The ending year denotes the rainy season; e.g., the annual rainfall of 1974/5 is attributed to 1975.

In addition, two variables are used to address the length of the rainy season; one is the "effective length," defined as the period between the dates in which 10% and 90% of the annual rainfall are accumulated, for the pertinent rainy season (following Paz and Kutiel 2003 and Reiser and Kutiel 2009). The other variable is the "Seasonality Index" (*SI*, Walsh and Lawler 1981), expressing the concentration of the rain with respect to the center of the season.

The synoptic definition of each rainy day was taken from the synoptic archive (available in Tel Aviv University), based on the method of Alpert et al. (2004a), which had been applied on the NCEP/NCAR reanalysis, with 2.5° × 2.5° resolution. This archive is used routinely for a wide spectrum of climate studies over the EM and Israel (e.g., Saaroni et al. 2010; Hochman et al. 2018a, b).

The Geopotential Height (GPH) at the 500–hPa level, used for calculating the MOI2 index (Palutikof 2003, see Section 2.2), together with the SST for the EM and the specific humidity (shum) at the 925-hPa level, expressing the Planetary Boundary Layer (PBL), was extracted from the NCEP-NCAR reanalysis data (Kalnay et al. 1996; Kistler et al. 2001). The SSTs were taken from 8 grid points included in the domain 31.4°N–35.23°N, 30.0°E–33.75 (excluding the point 35.23°N, 33.75°E, which is in Cyprus), corresponding to the EM. The specific humidity was taken from the grid point 32.5°N, 35°E, which represents the study area.

2.2 Methods

The individual stations were pooled into regions (Fig. 2), based on the "Ward" method, using the HiClimR R package (Ward 1963; Badr et al. 2015). This is an automatic clustering method, which divides observation points into a desired number of clusters, so that observations belonging to a certain cluster are the most similar with respect to a desired "sorting characteristic" and differ from those belonging to other clusters as much as possible. The clustering was applied on the IMS gridded rainfall data time series (1953–2017), with a 0.5-km resolution, sampled by taking each 5th point (total of 11,407 grid points), using the correlation between individual grid points as the sorting characteristic.

For each region, the representative rainfall, number of rainy days, average daily rainfall intensity, and the SI were the averages of the individual stations included in it. The "effective length" of the rainy season was calculated for each region separately, based on the daily rainfall time series, which was averaged over all stations included in the pertinent region. The
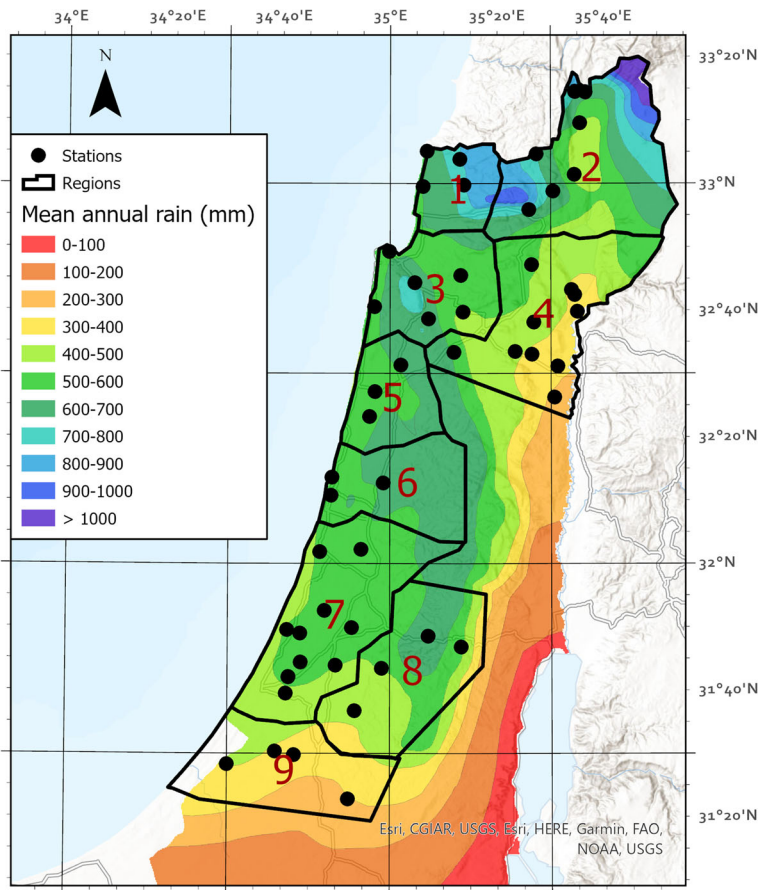

Fig. 2 Distribution of the rain stations and the regions, imposed on the map of the long-term mean annual rainfall over the study area (1981–2010, taken from the Israeli Meteorological Service, https://ims.gov.il/he/climateAtlas). The term "annual" refers to the "rainy season," which officially starts on 1 August and ends on 31 July. The 51 individual stations were pooled into nine regions (denoted by polygons), based on the "Ward" method, applying the HiClimR R package (Ward 1963; Badr et al. 2015)

advantage of this method is that it ignores the small amounts of rain that tend to occur at the beginning and end of the rainy season (Goldreich 2003), which have a small effect on soil water availability for plants, and therefore woody plants probably are less likely to respond to them.

The *SI* is defined by

$$SI = \frac{1}{R} \sum_{n=1}^{12} |x_n - R/12|, \tag{1}$$

where R is the annual rainfall, n is the serial number of the month (starting in this study from August, which officially denotes the beginning of the rainy season), and x_n is the monthly rainfall. Low *SI* reflects wider rainfall distribution, whereas high values (especially >1.0) reflect a narrow rainfall distribution, in which the rain is concentrated within less than half of the year. The *SI* circumvents the arbitrariness underlying the choice of the percentages denoting the beginning and ending of the rainy season in the definition of its effective length. This is especially important for the study area, in light of the local rains characterizing the beginning and end of the rainy season.

Two versions for the *SI* were proposed by Walsh and Lawler (1981). One ($\overline{SI}$) is based on a mean monthly and annual rainfall over a standard period, e.g., of 30 years. Here we used the rainy seasons 1981–2010. This version is useful for identifying the rain regime and for classifying the seasonal distribution. The other, denoted $\overline{SI_i}$, is the averaged over the SI_is, each calculated from the monthly and the annual rainfall of an individual rainy season (as implied by the subscript $_i$). Since the averaging of the individual monthly rainfall over years broadens the seasonal rainfall distribution, $\overline{SI}$ is larger than $\overline{SI_i}$ (Walsh and Lawler 1981). It should be noted that the effective length of individual rainy seasons and the SI_i are measures that better reflect the structure of the rainy season than monthly average rainfall distribution, since they are flexible and not confined to arbitrary dates.

In order to represent the effect of CLs on the inter-annual variation in the rainfall, we used three indices related to the CLs (CL variables, hereafter). One is the occurrences of CLs (number of CL days) according to the classification of Alpert et al. (2004a), second is the occurrence of deep CLs, and the third is a new index that combines the number of CL days and their intensity as a measure for their effect, named the Cyclonic Activity (CA) index. The CA value for a certain period is defined as:

$$CA = \sum_i \begin{cases} \text{if nondeep } CL \text{ exists} & 1 \\ \text{if a deep } CL \text{ exists} & \alpha \\ \text{else} & 0 \end{cases}, \tag{2}$$

where i is the serial number of the day and α (> 1) gives weight for the deep cyclones (see Section 3.5). The choice of $\alpha > 1$ stems from the higher rain yield of deep CLs compared to the other CLs (Saaroni et al. 2010).

The large-scale oscillation analyzed is the MOI2, defined as the 500-hPa geopotential difference between Gibraltar's Northern Frontier (36.1°N, 5.3°W) and Lod Airport in Israel (32.0°N, 34.5°E), following Palutikof (2003). As for the shum, the data representing the PBL was separated for the rainy days and non-rainy days. This separation exposed differences between the marine air currents, with which the rain in Israel is associated, and the arid air currents typifying a considerable part of the non-rainy days (Goldreich 2003). Hereafter, the 925-hPa shum of the rainy days was adopted as one of the rain-governing factors.

The relations between the rain governing factors (i.e., the three CL variables, the MOI2, the SST, and the shum) and the rain variables (i.e., total rainfall, number of rainy days, and daily average rainfall) were addressed in three ways. First, correlating each of the governing factors with each of the rain variables, for the various timescales. Second, estimating the contribution and significance of the governing factors, using a multi-regression analysis. Third, comparing the trends in the rain variables with the trends in the governing factors. Concerning the multi-regression analysis, we used a simple multiple regression model (regression model, hereafter, e.g., Sousa et al. 2011), using the SPSS software. The regression model aims to identify the significant factors explaining the inter-annual variations in the rain variables (predictand), based on a linear combination of the six factors (potential predictors). We applied the "backward regression" option, which starts the regression using all potential predictors and remove them one by one. The removal process continues as long as the variance explained (R^2) is not reduced beyond pre-defined threshold. According to the SPSS manual, this method is recommended when the number of predictors is smaller than the sample size and when predictors are correlated among each other, both true for the present study. The analysis was done for the entire study area and for each individual region, separately.

The trends in the variables specified above, and their statistical significance (two-tailed test), were calculated for the individual stations and regions, and are presented both as rates and as percentage of change, for part of them. The calculation of the slopes (trend rates) and their significance was done using the non-parametric method of Mann-Kendall's Tau correlation (τ) (Sen 1968), applying the R package (Pohlert 2020).

3 Results

3.1 Rain regime features

The annual rainfall, the number of rainy days, the average daily rainfall intensity, and the length of the rainy season for each of the 9 regions are presented in Table 1. The division of the study area to the nine regions is rather similar to the "geographical regions," defined by the IMS for climatological studies, and used for rainfall trend analysis by Ziv et al. (2014). A decrease in the annual rainfall and in the number of rainy days from north to south is clear, whereas no consistent spatial variations can be noted in the average daily rainfall intensity. The effective length of the rainy season is 112 days on average, and it shortens from north to south by 14 days (12.5%). The distribution of the long-term mean *SI* shows that the values range between 0.95 and 1.02, being <1.0 in the northern part of the study area and > 1.0 in the southern part. According to Walsh and Lawler (1981), Israel is divided between the lower margins of "Markedly seasonal with a long dry season" in the north, and the higher margins of "most rain in 3 months, or less," in the south.

The long-term monthly mean rainfall for each of the 9 regions is presented in Fig. 3. It demonstrates the peak rainfall in the mid-winter months (DJF) and the decrease from north to south. The ratio between the rainfall in the northernmost regions (no. 1 and no. 2), and the southernmost one (no. 9) for the various months varies between 1.6 and 3.2, with an average of 2.0.

3.2 Trends in the annual rainfall, number of rainy days, and daily rainfall intensity

The annual rainfall during the study period (1975–2020) is shown to have no trend, whereas the number of rainy days has a decreasing trend, and the average daily rainfall intensity is

Table 1 Long-term mean annual rainfall (mm), number of rainy days (≥ 1 mm), average daily rainfall intensity (mm/day), average date of the beginning and end of the rainy season (10% and 90% rain accumulation, respectively), the effective length of the rainy season (no. of days), and the $\overline{SI}$ for each of the regions (denoted in Fig. 2) and for the entire study area. The data is calculated for the study period (1975–2020), except the $\overline{SI}$, which is based on a standard 30-year period (1981–2010), since its value depends on the length of the period used for its derivation

Region	Annual rainfall (mm)	No. of rainy days	Daily rainfall intensity (mm/day)	Date of 10% accumulation	Date of 90% accumulation	Effective length (no. of days)	$\overline{SI}$
1	707	55	10.6	18-Nov	16-Mar	119	0.95
2	639	53	9.8	20-Nov	19-Mar	119	0.98
3	603	50	10.0	20-Nov	14-Mar	114	0.99
4	408	43	7.8	22-Nov	18-Mar	116	0.99
5	584	49	10.0	20-Nov	10-Mar	110	0.99
6	552	46	10.1	18-Nov	7-Mar	109	0.99
7	522	40	10.5	21-Nov	8-Mar	107	1.01
8	525	41	10.0	25-Nov	15-Mar	110	1.02
9	360	34	8.6	26-Nov	11-Mar	105	1.02
Avg.	**545±139**	**46±8.5**	**9.6±1.3**	**21-Nov**	**13-Mar**	**112±18**	**0.99**

increasing (Fig. 4). The annual rainfall has no consistent trend among the individual stations and regions (Fig. 4(a, d)). For the number of rainy days (Fig. 4(b, e)), the trends are negative in all the individual stations and regions, significant only in 3 of the stations (Fig. 4(b)). Since the trends in the individual stations are highly variable, and produce a noisy field, we hereafter focus on the regional scale, which shows negative trends, at an average rate of −0.87 days/decade (−1.9%/decade). The trend of the average daily rainfall intensity (Fig. 4(c, f)) shows an increase in eight out of the nine regions, at an average rate of +0.24 mm/day/decade (+2.0%/decade), with a general increase from south to north, statistically significant in the northwestern region. As for the individual stations (Fig. 4(c)), the trend is positive in their vast majority, statistically significant in 4 of them.

3.3 Trends in the intra-seasonal timescale

The intra-seasonal trends in the rainfall, indicating an increase in the mid-winter (DJF) and a decrease in the autumn (SON) and spring (MAM), are shown in Fig. 5. The average trend of
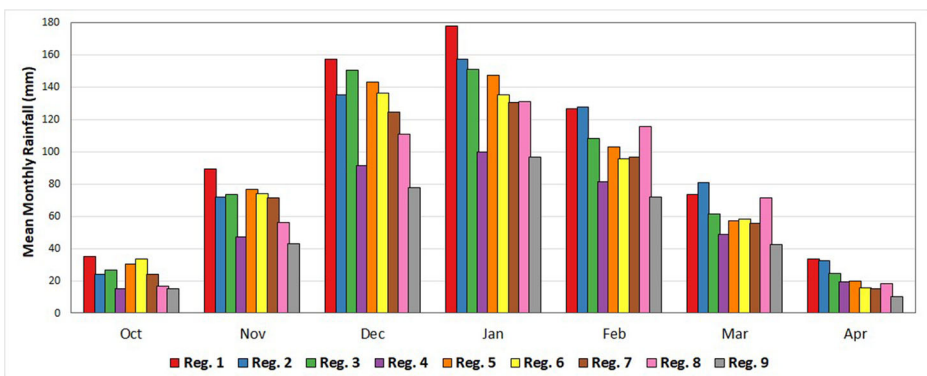

Fig. 3 Long-term monthly mean rainfall for each of the 9 regions (mm, bars)
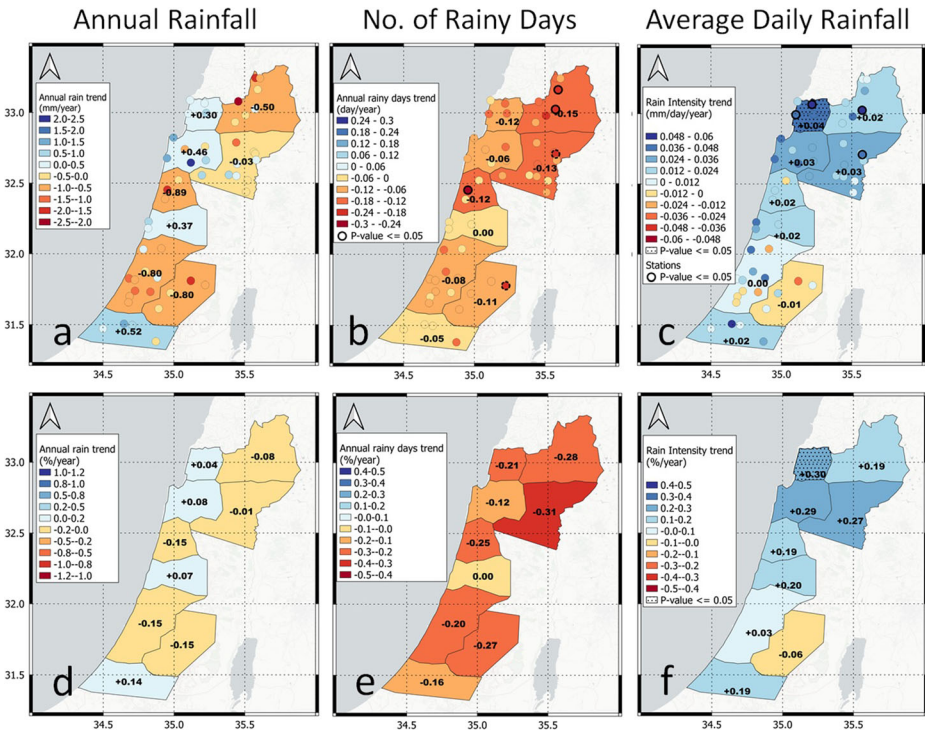
Fig. 4 Long-term linear trend of the annual rainfall, in mm/year units (a), of the number of rainy days, in days/year units (b), of the daily rainfall intensity, in mm/day units (c), and their respective percent change (%, d, e, and f) for the study period, 1975–2020. Stations in which the trends are significant at the 0.05 level are denoted by black circles and regions in which the trends are significant are dotted

DJF rainfall (Fig. 5(b)) is +13.5 mm/decade (+3.7%/decade), and the respective values for the transitional seasons, SON and MAM (Fig. 5(a, c)), are −3.1 and − 6.6 mm/decade (−3.3% and − 7.6%/decade). None of these trends is statistically significant. The trend of the number of rainy days (Fig. 5(d–f)) is negative in all parts of the rainy season. The average rates are −0.14, −0.48, and − 0.31 days/decade, which are −1.8%, −1.7%, and − 3.1%/decade for SON, DJF, and MAM, respectively, but all are statistically insignificant.

The trends in the daily average rainfall intensity have the same course as that of the rainfall (compare the lower to the upper panel of Fig. 5). In the mid-winter (DJF), the increasing trend in the daily intensity ranges between +1.5 and + 6.4%/decade (Fig. 5(h)). The largest increases are in the north of the study area, being statistically significant in five regions. For SON, the trends are negative in eight of the regions, ranging between −4.3 and − 8.2%/decade, and positive only in the southernmost region (Fig. 5(g)). The negative trend is the largest in the Judean Mountains, where it is statistically significant, and in the northeastern region. For MAM, all trends are negative, ranging between −3.6 and − 9.3%/decade, statistically significant in four regions, located in the northern part of the study area and in the Judean Mountains (Fig. 5(i)).

The rainfall trends for the individual months indicate that changes in three of the months lead the intra-seasonal trends: November, January, and March (Fig. 6). A distinct seasonal course is noted, with a negative trend in October–December, a positive trend in January (significant in the two coastal regions in the northern part of the study area), and negative in
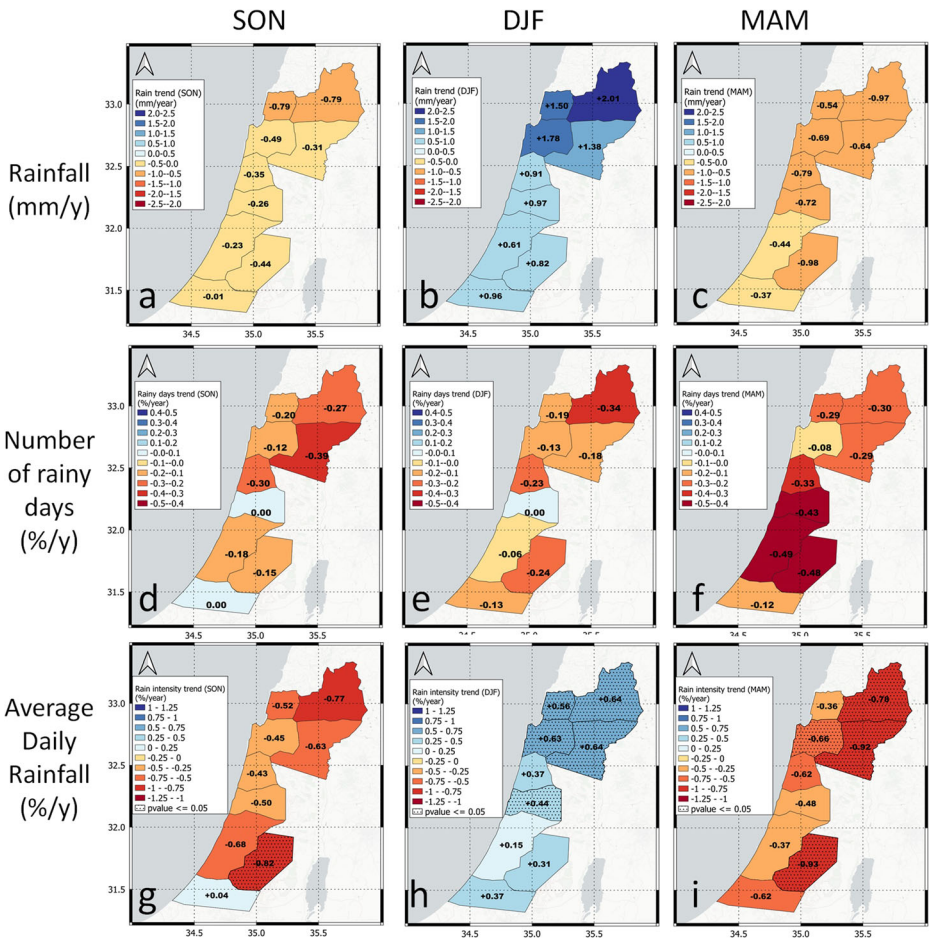
Fig. 5 Long-term linear trend of the intra-seasonal rainfall (upper panel, mm/year), number of rainy days (medium panel, %/year), and of the daily rainfall intensity (lower panel, %/year), for September–November (a, d, and g), December–February (b, e, and h) and March–May (c, f, and i). Regions in which the trends are significant are dotted

March (significant in 5 of the regions). Note the symmetric structure of the trends with respect to January, the mid-winter month.

3.4 Trends in the length of the rainy season

The "effective length" of the rainy period is shortening in all regions (Fig. 7), without being statistically significant. For the 10% date, a progression is seen in seven out of the nine regions, with a maximum rate of 2.3 days/decade, whereas a slight regress appears in the southwest regions (Fig. 7(a)). The trend of the 90% date (Fig. 7(b)) resembles a "mirror image" of that for the 10%. The southwest regions show the largest regression, against a progression in the four northernmost regions. Note that the progression of the 10% date has the same implication as the retrogression of the 90% date, i.e., a shortening of the effective rainy season. Therefore, the color tables of Fig. 7(a, b) are reversed with respect to each other. The trend of the effective
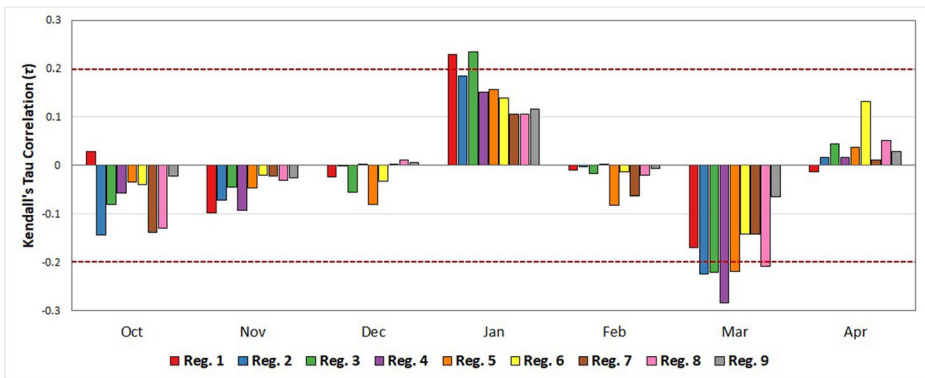
Fig. 6 Kendall's Tau correlation (τ) with linear trend of the monthly rainfall variation, in each of the 9 regions, for the study period (1975–2020). The borders of the 0.05 significance level (±0.20) are marked by dashed red lines

length of the rainy season (Fig. 7(c)) is negative (shortening) over most of the study area, at an average rate of −1.59 days/decade, i.e., −7.3 days (−6.5%) during the 46 years of the study period.

The seasonality index (*SI*) has increased in the vast majority of the study area, implying a general contraction of the rainy season. The long-term trend of the SI_i (Fig. 8) indicates an increase at an average rate of +0.016/decade, i.e., +7% during the study period. The trend is statistically significant in the Judean Mountains.

3.5 The contribution of the governing factors

The inter-annual variations of the rainfall, the number of rainy days, and the daily rainfall intensity were found significantly correlated with the synoptic factors, i.e., the three CL variables and the MOI2 (Table 2), mostly the CA index, but not with the SST and the shum. The correlations between the rain variables, averaged over the entire study area, and the CA are +0.63 with the annual rainfall, +0.64 with the number of rainy days, and + 0.27 with the
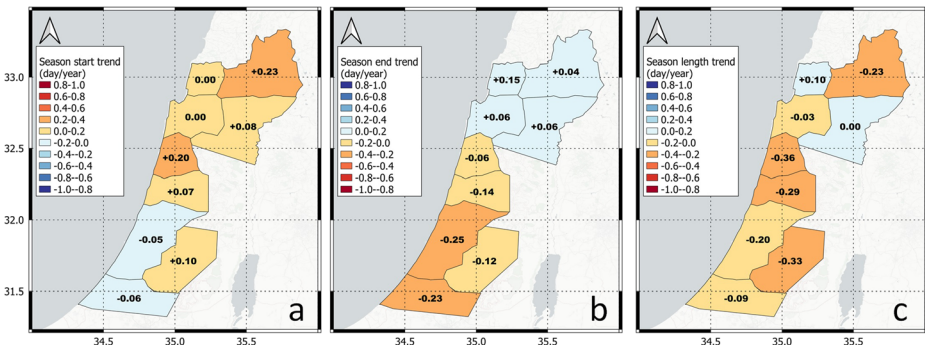

Fig. 7 Long-term linear trend of the date in which 10% of the annual rainfall is accumulated (a), the date in which 90% of the annual rainfall is accumulated (b), and the "effective length" of the rainy season (c) along the study period (1975–2020), all in days/year. The coloring of the trend in each map refers to the implied trend of the effective length of the rainy season. Trends reflecting shortening of the season are colored in warm colors and these implying its lengthening are in cold colors. Therefore, the color tables of Fig. 7(a, b) are reversed with respect to each other

Fig. 8 The long-term linear trend of SI_i along the study period (1975–2020). Regions in which the trends are significant at the 0.05 level are dotted
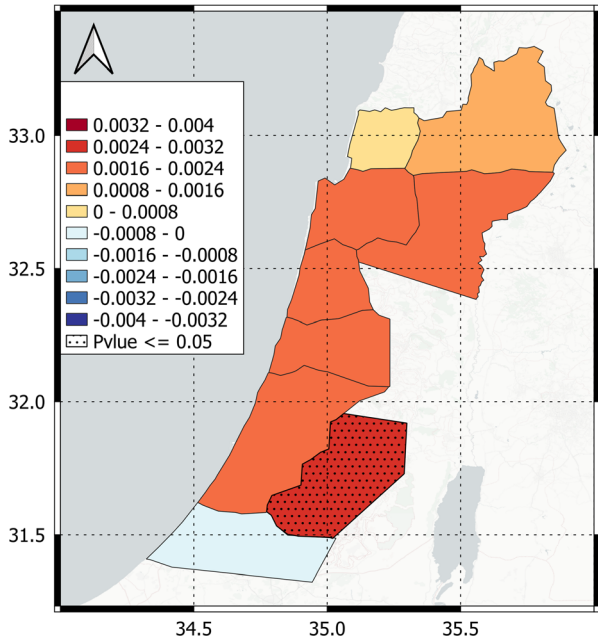
daily rainfall intensity. The highest correlation between the CA index and the rainfall was obtained when α (the multiplier of the number of deep CLs in Eq. 2) was set to 2.0, after all values between 1.1 and 3.0 were examined. The correlations between the rain variables and the synoptic factors (CA, CLs, deep CLs, and MOI2) are all positive (significant at the 0.05 level) and these with the shum are all negative, but small and insignificant. As for the SST, it is significantly positively correlated with the shum ($R = + 0.57$) and with the synoptic factors. Its correlation with the rainfall and with the number of rainy days is negative, being significant for the latter.

On the regional scale (not shown), the correlations of the annual rainfall with all variables are significant, except with the shum. The correlation of the CA, the CLs, and the deep CLs' occurrence with the three rain variables decreases from north to south, whereas these of the MOI2 increases from north to south. No consistent spatial trend is noted for the correlations with the SST and the shum.

A multi-regression analysis between the governing factors and each of the rain variables shows that the CA is the dominant factor (see Table 3 and Appendix A). On the regional scale, the variance explained by the factors found significant varies between 37 and 67% for the annual rainfall, 44 and 72% for the number of rainy days, and 0–28% for the daily rainfall intensity. The variance explained keeps high values over the north and central parts of the study area and drops sharply in the southernmost region. For the annual rainfall and the number of rainy days, the CA is the only significant factor in most of the regions, whereas in the southern regions the MOI2 is also significant. For the daily rainfall intensity, the role of the significant factor shifts between the CA and the other two CL indices, whereas for the southernmost region no significant factor was found.

The long-term trend of the two variables reflecting thermodynamic factors, the SST and the shum, show a significant increase, whereas the two indices representing synoptic factors, the

Table 2 Correlations (R) between the rain variables (annual rainfall, number of rainy days and daily rainfall intensity) and the SST, 925-hPa shum in the rainy days, occurrence of CLs and deep CLs, CA index, and MOI2, together with the correlation between the environmental factors. Correlations significant at the 0.05 level are bold

	SST	shum	CLs	Deep CLs	CA	MOI2
Annual rainfall	−0.18	−0.08	**+0.55**	**+0.53**	**+0.63**	**+0.37**
Rainy days	**−0.25**	−0.08	**+0.60**	**+0.49**	**+0.64**	**+0.41**
Daily rainfall intensity	+0.02	−0.10	**+0.21**	**+0.27**	**+0.27**	+0.16
SST	1	**+0.57**	**−0.36**	−0.22	**−0.34**	**−0.34**
Shum		1	−0.12	−0.18	−0.15	−0.25
CLs			1	**+0.64**	**+0.96**	**+0.53**
Deep CLs				1	**+0.82**	**+0.41**
CA					1	**+0.53**

CA and the MOI2, show no significant trends, mostly negative (Fig. 9). The SST is the only variable having a significant positive trend in all months. Second is the shum, having positive trend in all months, except January, statistically significant in November and December and at the annual timescale. As for the rain variables, their trends fluctuate in a manner that does not correspond to that of the thermodynamic variables. However, the positive trend found in the three rain variables in January and the negative trends found in November and March have the same signs as the trends in the synoptic factors, the CA and the MOI2.

4 Discussion

The present study, covering the 46 years from the beginning of persisting global warming up to 2020, is the first that does not support the drying trend, projected by the climate models and found in previous observational studies for Israel, by showing an absence of rainfall trend. Examination of the two rainfall ingredients, the number of rainy days and the daily rainfall intensity, revealed contradicting trends, each goes in line with future projections (e.g., IPCC 2018; Hochman et al. 2018c). First is the reduction in the number of rainy days, found in all 9 regions, at an average rate of −1.9%/decade (though statistically insignificant). Second is the daily rainfall intensity, found to increase, at an average rate of +2.0%/decade, being significant in one of the regions and marginally (at the 0.1 level) in other 2 regions. Following previous studies of trends in the rain regime in the Levant (e.g., Shohami et al. 2011; Yosef et al. 2019), we find it important to refer to trends even when their significance is marginal. This stems from the high vulnerability of the region and due to the high natural variability of the rain variables in the study area, as argued by Morin (2011).

The decreasing trend in the number of the number of rainy days agrees with Ziv et al. (2014) and with Yosef et al. (2019). The increase in the daily rainfall intensity agrees with that found by Alpert et al. (2002) for 1951–1995 and with Yosef et al. (2009) for 1951–2004. It agrees also with Yosef et al. (2019), who used a "simple daily intensity index" (SDII), which is the "annual total precipitation divided by the number of wet days," and showed an increase (though statistically insignificant) for both 1950–2017 and 1988–2017 periods.

The intra seasonal analysis indicates a substantial difference between the mid-winter, which has become wetter, and its two ends, becoming drier. A positive trend in both the rainfall intensity (significant in 5 out of the 9 regions) and the rainfall (not significant) was found in DJF and negative in the transitional seasons (significant in 4 and 1 regions in SON and MAM,

Table 3 The variables found as significant predictors for the rain variables on the annual timescale, for each region, and for the entire study area. Calculated by the regression model (Sousa et al. [2011]), using the SPSS software, applying the "backward regression" option as significant. The potential predictors are the CL variables (CLs and deep CLs occurrence, and the CA index), the MOI2, the SST, and the 925-hPa shum in rainy days

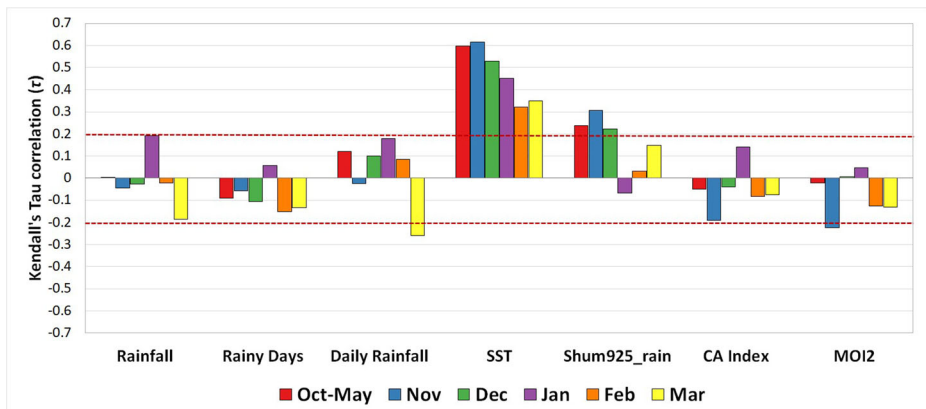| Region	Rainfall		No. of rainy days		Daily rainfall intensity	
	Sig. factors	Var. explained (%)	Sig. factors	Var. explained (%)	Sig. factors	Var. explained (%)
1	CA	63	CA	61	Deep CLs, SST	24
2	CA, Deep CLs	67	CA	63	Deep CLs	28
3	CA	62	CA	67	CA	14
4	CA	61	CA	66	CA, SST	10
5	CA	55	CA	59	CA	8
6	CA, MOI2	68	CA, MOI2	72	CA	18
7	CA, MOI2	64	CA, MOI2	59	CA	10
8	CA, MOI2	59	CA, MOI2	58	Shum 925	5
9	MOI2, CA	37	MOI2, CA	44	None	0
Study area	**CA, MOI2**	**71**	**CA, MOI2**	**67**	**CA**	**13**

Fig. 9 Kendall's Tau correlation (τ) with linear trend (1975–2020) of the following variables: rainfall, number of rainy days, daily rainfall intensity, SST, 925-hPa specific humidity (shum) for rainy days, the CA index, and the MOI2. For each variable, the correlation is presented for the rainy season (Oct–May), and for the individual months: Nov, Dec, Jan, Feb, and Mar (bars). The borders of the 0.05 significance level (±0.20) are marked by dashed red lines. The trends in the CLs and deep CLs (not shown) are similar to that of the CA index

respectively). The increase in the daily rainfall intensity in DJF overrides the reduction in the number of rainy days in these months, yielding the rainfall positive trend. During the ends of the rainy season, both the daily rainfall intensity and the number of rainy days decrease, yielding the rainfall decrease. This intra-seasonal course contradicts the negative rainfall trends, found for all parts of the rainy season by Shohami et al. (2011), presumably due to their choice of only one rain station and the different study period they referred to (1965–2003). The positive trend in the daily rainfall intensity in DJF is the largest in the northern regions, at rates on the order of ~3%/decade. These regions are the rainiest in the study region. This, together with the fact that the daily rainfall intensity in DJF in these regions is higher than that in the autumn and spring (11.7, 9.0, and 7.6 mm/day, respectively), stresses the exacerbated risk of flooding. This subject is noted by the IPCC (2018).

The analysis on the monthly timescale revealed that the rainfall increase in DJF is dominated by January (significant in 2 regions and marginally in another one), at a rate that is equivalent to 2.4% of the annual rainfall per decade. The respective rates for November and March are −0.6% and −1.6% (significant in 5 regions in March). The decline found for November was expressed by extremely dry Novembers in 2010, 2013, 2016, and 2019 (Porat 2016, 2019), resulting in two major fires, one in 2010 (Malkinson 2012) and another in 2016, beyond vast environmental impacts such as on water shortage and extension of the irrigation period.

The increase in the rainfall in the middle of the rainy season, on the account of its two ends, reflects a contraction trend of the rainy season, which effective length is less than 4 months in the study area (Table 1). The $\overline{SI}$ increases from north to south, indicating that the rainy season in north Israel is longer than that in the south, in agreement with the 14-day difference in its effective length in favor of the north and with Goldreich (2003). The increase in the SI_i during the study period (statistically significant in one region and marginally in another one) indicates that the study area is shifting from "markedly seasonal with a long dry season" toward "most rain in 3 months, or less." The "effective length" of the rainy season, being 112 days on the average, has shortened at a rate of −1.59 days/decade, i.e., 7.3 days during the 46 years. This rate is half of that found by Ziv et al. (2014) for the period 1975–2010.

The combined contributions of the synoptic and the thermodynamic factors partly explain the intra-seasonal course of the rainfall trend. The synoptic factors, which were found highly correlated with the rainfall, the CA and MOI2, in agreement with Saaroni et al. (2010) and Ziv et al. (2014), showed an increase in January and a considerable decrease in November. However, the trends in the synoptic factors cannot explain the absence of a trend in the annual rainfall. As for the thermodynamic factors, they show negative correlations with the rainfall, marginally significant for the SST (Table 2), in contrast with the expected positive contribution to the rainfall (implied by the IPCC 2018). We hypothesize that in spite of this negative correlation, the significant positive trend in the thermodynamic factors may explain why, despite the negative average trend in the synoptic factors, there is no trend in the rainfall. In addition, it can also explain the increase in the daily rainfall intensity on the annual timescale.

The negative correlation between the SST and the rainfall on the inter-annual timescale reflects an interaction between the CLs and the EM, which masks the long-term positive relation expected to exist between them. This negative correlation reflects the heat extraction from the sea surface via sensible and latent heat fluxes from the sea surface to the overlying cold air masses, which are transported by the CLs while passing over the EM (Shay-El and Alpert 1991). Hence, above-normal rainy seasons are expected to be associated with lower SST. This is supported by the "remarkable correlation" between the heat storage depletion in the EM during the rainy season and the annual rainfall in Israel, found by Tzvetkov and Assaf (1982). The factor that might explain the low SST-rainfall correlation found in the present study is the positive correlation between the heat storage in the EM prior to the rainy season and the annual rainfall in Israel, shown also by Tzvetkov and Assaf (1982). It is worth noting that in the process underlying the long-term positive correlation between the heat storage and the rainfall is thermodynamic, i.e., the SST, whereas the factor leading the inter-annual positive correlation between the heat depletion and the rainfall is synoptic, represented here by the CA index.

On the regional scale, the multi-regression analysis indicates that the CA is the only significant factor affecting the annual rainfall and the number of rainy days in the northern regions, and the MOI2, secondary to the CA, is significant in the 3 and 4 southernmost regions for the annual rainfall and the number of rainy days, respectively. The MOI2 was previously shown to be correlated with the rainfall over the study area by Ziv et al. (2014), but the present study is the first to assess spatial variations in its impact. The sensitivity of the rainfall in south Israel to the MOI2 can be deduced from the linkage between this index and the circulation pattern over the Mediterranean. A positive MOI2 implies a southward shift of the upper level isohypses over the EM, leading to a southward shift of the CL tracks, which enhances their influence on south Israel. This effect is minor for north Israel, which is almost always close to the average CL track, located north of the study area (e.g., Alpert et al. 1990).

The reduction in the cyclonic activity in the transitional seasons can be attributed to the enhanced influence of the descending branch of the Hadley cell due to its northward expansion (Lu et al. 2007; Previdi and Liepert 2007; Seidel et al. 2008; Johanson and Fu 2009; Seager et al. 2010). The seasonal oscillation of the Hadley cell implies that its descending branch is at its southernmost location in the mid-winter. Thus, even if it shifts northward, its effect on the Mediterranean is still expected to remain minor. However, in the transitional seasons, the descending branch approaches the Mediterranean, so any northward shift implies further suppression in the CLs' activity. This explains the reduction in the synoptic factors and the rain variables during the transitional seasons. The resulting climatic change is the contraction of the rainy season or elongation of the long dry (rainless) season.

5 Summary and conclusions

The present study analyzes trends in the annual rainfall, number of rainy days, and daily rainfall intensity, which constitute the rain regime, in the part of Israel having Mediterranean and semi-arid climate. The need for studying these trends as of today stems from the proximity of this region to the subtropical desert belt and from the alarming future projections of rainfall decrease over the Mediterranean, on the order of tens of percent toward the end of the twenty-first century. Several recent studies have confirmed the expected drying, though none of them found it statistically significant. The present study, covering the period 1975–2020, during which global warming is persistent, indicates no trend in the annual rainfall. The absence of any trend in the annual rainfall reflects an offset between a decline in the number of rainy days, and an increase in the average daily rainfall intensity, both at a rate of ~2%/ decade. The observed trends in the number of rainy days and in the daily rainfall intensity agree in their signs with those projected for the future by the climate models, but not in their magnitudes.

The trends in the synoptic factors, reflected by the CLs' activity and the MOI2, were found negative, whereas the thermodynamic factors, the shum and the SST, were found positive, significant only for the SST. However, multi-regression analyses indicated that the CA, a synoptic factor developed in this study to represent the CLs' activity, is the only significant factor for the rainfall and for the number of rainy days in the northern part of the study area. Another synoptic factor, the MOI2, was found as an additional factor influencing rainfall in the southern part of the study area.

The most pronounced finding is a change in the structure of the rainy season: rainfall increase in the mid-season (DJF, primarily in January) and decrease in both its ends (SON and MAM). Analysis of the contributors for this change shows that while the number of rainy days has declined along the entire rainy season, the daily rainfall intensity declined during autumn and spring and increased in the mid-winter. The above trends reflect a contraction of the rainy season. It is expressed in a shortening of the "effective length" of the rainy season (112 days on the average), at a rate of −1.5 days/decade, and in an increase of the seasonality index (*SI*). According the definition of Walsh and Lawler (1981), this implies that the climate in Israel is shifting from being at the border between "markedly seasonal with a long dry season" and "most rain in 3 months, or less" further toward the latter regime.

It is proposed that the rain decline in the transitional seasons results from the increasing influence of the descending branch of the Hadley cell in the margins of the rainy season. The daily rainfall intensity increase in the mid-winter may result from the increase found in the SST over the EM, the moisture source of rain in Israel. Unfortunately, the multi-regression analysis could not resolve this effect, suggesting the use of numerical simulations for this end.

Changes in the rain regime and in the structure of the rainy season have vast human and ecosystem impacts, such as increase in flood risks, shortage of water, increase in irrigation demands, and enhanced risk of fires. Mediterranean vegetation had thousands of years to adapt to the seasonal climate but may not be able to re-adapt rapidly to the extremely short new season, as exemplified in forest mortality events (Carnicer et al. 2011; Sarris et al. 2011). Furthermore, the increasing rainfall concentrated in the mid-winter months can further decrease the efficiency of such rainy days due to severe flooding and loss of rainfall that can no longer effectively infiltrate into the soil or be used by plants.

Appendix

The prediction equations for the annual rainfall, number of rainy days, and daily rainfall intensity, together with the normalized coefficients (Betas) are presented in Table 4. The predictors are specified in Section 2.

Table 4 Regression equations and normalized coefficients for the rain variables

	Annual rainfall	**Number of rainy days**	**Daily rainfall intensity**
Equation	$-26.954 + 7.612\,CA + 1.203\,MOI2$	$12.340 + 0.443\,CA + 0.081\,MOI2$	$8.530 + 0.045\,CA$
Beta	For CA: 0.745, for MOI2: 0.174	For CA: 0.708, for MOI2: 0.192	For CA: 0.389

References

Alpert P, Neeman BU, Shay-El Y (1990) Climatological analysis of Mediterranean cyclones using ECMWF data. Tellus 42A:65–77

Alpert P, Ben-Gai T, Baharad A, Benjamini Y, Yekutieli D, Colacino M, Diodato L, Ramis C, Homar V, Romero R, Michaelides S, Manes A (2002) Evidence for increase of extreme daily rainfall in the Mediterranean in spite of decrease in Total values. Geophys Res Lett 29(1536):31–34. https://doi.org/10.1029/2001GL013554

Alpert P, Osetinsky I, Ziv B, Shafir H (2004a) Semi-objective classification for daily synoptic systems: application to the eastern Mediterranean climate change. Int J Climatol 24(8):1001–1011

Alpert P, Osetinsky I, Ziv B, Shafir H (2004b) A new seasons definition based on classified daily synoptic systems: an example for the eastern Mediterranean. Int J Climatol 24(8):1013–1021

Alpert P, Price C, Krichak SO, Ziv B, Saaroni H, Osetinsky I, Barkan J, Kishcha P (2005) Tropical tele-connections to the Mediterranean climate and weather. Adv Geosci 2:157–160

Alpert P, Krichak SO, Shafir H, Haim D, Osetinsky I (2008) Climatic trends to extremes employing regional modeling and statistical interpretation over the E. Mediterranean. Glob Planet Chang 63:163–170

Badr HS, Zaitchik BF, Dezfuli AK (2015) A tool for hierarchical climate regionalization. Earth Sci Inf 8:949–958

Blondel J, Aronson J, Bodiou JY, Boeuf G (2010) The Mediterranean region: biological diversity in space and time. Oxford University Press, Oxford

Carnicer J, Coll M, Ninyerola M, Pons X, Sanchez G, Penuelas J (2011) Widespread crown condition decline, food web disruption, and amplified tree mortality with increased climate change-type drought. Proc Natl Acad Sci 108(4):1474–1478

Chenoweth J, Hadjinicolaou P, Bruggeman A, Lelieveld J, Levin Z, Lange MA, Xoplaki E, Hadjikakou M (2011) Impact of climate change on the water resources of the eastern Mediterranean and Middle East region: modeled 21st century changes and implications. Water Resour Res 47:W06506. https://doi.org/10.1029/2010WR010269

de Vries AJ, Tyrlis E, Edry D, Krichak SO, Steil B, Lelieveld J (2013) Extreme precipitation events in the Middle East: dynamics of the Active Red Sea Trough. J Geophys Res-Atmos 118(13):7087–7108

Giorgi G, Lionello P (2008) Climate change projections for the Mediterranean region. Glob Planet Chang 63:90–104

Goldreich Y (2003) The climate of Israel: observation, research and application. Kluwer Academic Publishes, New York

Goldreich Y, Moses H, Rosenfeld D (2004) Radar analysis of cloud systems and their rainfall yield in Israel. Isr J Earth Sci 53:63–76

Hochman A, Harpaz T, Saaroni H, Alpert P (2018a) Synoptic classification in 21st century CMIP5 predictions over the eastern Mediterranean with focus on cyclones. Int J Climatol 38(3):1476–1483. https://doi.org/10.1002/joc.5260

Hochman A, Harpaz T, Saaroni H, Alpert P (2018b) The seasons' length in 21st century CMIP5 projections over the eastern Mediterranean. Int J Climatol 38(6):2627–2637. https://doi.org/10.1002/joc.5448

Hochman A, Mercogliano P, Alpert P, Saaroni H, Bucchignani E (2018c) High resolution projection of climate change and extremity over Israel using COSMO-CLM. Int J Climatol 38(14):5095–5106. https://doi.org/10.1002/joc.5714

Hoegh-Guldberg O, Jacob D, Taylor M, Bindi M, Brown S, Camilloni I, Diedhiou A, Djalante R, Ebi KL, Engelbrecht F, Guiot J, Hijioka Y, Mehrotra S, Payne A, Seneviratne SI, Thomas A, Warren R, Zhou G (2018) Impacts of 1.5°C global warming on natural and human systems. In: Masson-Delmotte V, Zhai P, Pörtner HO et al (eds) Global Warming of 1.5°C, An IPCC Special Report on the impacts of global warming of 1.5°C above pre-industrial levels and related global greenhouse gas emission pathways, in the context of strengthening the global response to the threat of climate change, sustainable development, and efforts to eradicate poverty In Press

Johanson CM, Fu Q (2009) Hadley cell widening: model simulations versus observations. J Clim 22:2713–2725

Kalnay E, Kanamitsu M, Kistler R, Collins W, Deaven D, Gandin L, Iredell M, Saha S, White G, Woollen J, Zhu Y, Leetmaa A, Reynolds R, Chelliah M, Ebisuzaki W, Higgins W, Janowiak J, Mo KC, Ropelewski C, Wang J, Jenne R, Joseph D (1996) The NCEP/NCAR 40-year reanalysis project. Bull Am Meteorol Soc 77:437–471

Kelley CP, Mohtadi S, Cane MA, Seager R, Kushnir Y (2015) Climate change in the Fertile Crescent and implications of the recent Syrian drought. Proc Nat Acad Sci USA 112(11):3241–3246

Kistler R, Kalnay E, Collins W, Saha S, White G, Woollen J, Chelliah M, Ebisuzaki W, Kanamitsu M, Kousky V, van den Dool H, Jenne R, Fiorino M (2001) The NCEP-NCAR 50-year reanalysis: monthly means CD-ROM and documentation. Bull Am Meteorol Soc 82:247–267

Kostopoulou E, Jones PD (2005) Assessment of climate extremes in the Eastern Mediterranean. Meteorog Atmos Phys 89:69–85

Krichak SO, Feldstein SB, Alpert P, Gualdi S, Scoccimarro E, Yano JI (2015) Discussing the role of tropical and subtropical moisture sources in extreme precipitation events in the Mediterranean region from a climate change perspective. Nat Hazards Earth Syst Sci Discuss 3:3983–4005

Lelieveld J, Hadjinicolaou P, Kostopoulou E, Chenoweth J, El Maayar M, Giannakopoulos C, Hannides C, Lange MA, Tanarhte M, Tyrlis E, Xoplaki E (2012) Climate change and impacts in the Eastern Mediterranean and the Middle East. Clim Chang 114:667–687

Lionello P, Giorgi F (2007) Winter precipitation and cyclones in the Mediterranean region: future climate scenarios in a regional simulation. Adv Geosci 12:153–158

Lu J, Vecchi GA, Reichler T (2007) Expansion of the Hadley cell under global warming. Geophys Res Lett 34: L06805. https://doi.org/10.1029/2006GL028443

Malkinson D (2012) Wildfire heterogeneity: empirical vs. simulated observations – the Carmel 2010 wildfire as a case study. Isr J Ecol Evol 58(2–3):165–176

Morin E (2011) To know what we cannot know: global mapping of minimal detectable absolute trends in annual precipitation. Water Resour Res 47:W07505. https://doi.org/10.1029/2010WR009798

Palutikof JP (2003) Analysis of Mediterranean climate data: measured and modelled. In: Bolle HJ (ed) Mediterranean climate: variability and trends. Springer-Verlag, Berlin

Paz S, Kutiel H (2003) Rainfall regime uncertainty (RRU) in an eastern Mediterranean region—a methodological approach. Isr J Earth Sci 52:47–63

Pohlert T (2020) Trend: non-parametric trend tests and change-point detection. R package version 1.1.2. https://CRAN.R-project.org/package=trend

Porat A (2016) Monthly weather summary – November 2016. IMS publication, December 2016 (in Hebrew) https://ims.gov.il/sites/default/files/nov16.pdf

Porat A (2019) Monthly weather summary – November 2016. IMS publication, December 2019 (in Hebrew) https://ims.gov.il/sites/default/files/nov19_1.pdf

Previdi M, Liepert B (2007) Annual modes and Hadley cell expansion under global warming. Geophys Res Lett 34(22):L22701. https://doi.org/10.1029/2007GL031243

Raible CC, Ziv B, Saaroni H, Wild M (2010) Winter synoptic-scale variability over the Mediterranean Basin under future climate conditions as simulated by the ECHAM5. Clim Dyn 35:473–488. https://doi.org/10.1007/s00382-009-0678-5

Raymond F, Ullmann A, Camberlin P, Oueslati B, Drobinski P (2018) Atmospheric conditions and weather regimes associated with extreme winter dry spells over the Mediterranean Basin. Clim Dyn 50(11–12): 4437–4453. https://doi.org/10.1007/s00382-017-3884-6

Reiser H, Kutiel H (2009) Rainfall uncertainty in the Mediterranean: definitions of the daily rainfall threshold (DRT) and the rainy season length (RSL). Theor Appl Climatol 97:151–162. https://doi.org/10.1007/s00704-008-0055-z

Rubin S, Ziv B, Paldor N (2007) Tropical plumes over eastern North Africa as a source of rain in the Middle East. Mon Weather Rev 135:4135–4148

Saaroni H, Halfon H, Ziv B, Alpert P, Kutiel H (2010) Links between the rainfall regime in Israel and location and intensity of Cyprus Lows. Int J Climatol 30:1014–1025. https://doi.org/10.1002/joc.1912

Samuels R, Hochman A, Baharad A, Givati A, Levi Y, Yosef Y, Saaroni H, Ziv B, Harpaz T, Alpert P (2017) Evaluation and projection of extreme precipitation indices in the Eastern Mediterranean based on CMIP5 multi model ensemble. Int J Climatol 38(5):2280–2297. https://doi.org/10.1002/joc.5334

Sarris D, Christodoulakis D, Körner C (2011) Impact of recent climatic change on growth of low elevation eastern Mediterranean forest trees. Clim Chang 106(2):203–223

Schlaepfer DR, Bradford JB, Lauenroth WK, Munson SM, Tietjen B, Hall SA, Wilson SD, Duniway MC, Jia G, Pyke DA, Lkhagva A (2017) Climate change reduces extent of temperate drylands and intensifies drought in deep soils. Nat Commun 8(1):1–9

Seager R, Naik N, Vecchi GA (2010) Thermodynamic and dynamic mechanisms for large-scale changes in the hydrological cycle in response to global warming. J Clim 23(17):4651–4668

Seidel DJ, Fu Q, Randel WJ, Reichler TJ (2008) Widening of the tropical belt in a changing climate. Nat Geosci 1:21–24

Sen PK (1968) Estimates of the regression coefficient based on Kendall's tau. J Am Stat Assoc 63(324):1379–1389. https://doi.org/10.1080/01621459.1968.10480934

Shalev S, Saaroni H, Izsak T, Yair Y, Ziv B (2011) The spatio-temporal distribution of lightning over Israel and the neighboring area and its relation to regional synoptic systems. Nat Hazards Earth Syst Sci Discuss 11:2125–2135. https://doi.org/10.5194/nhess-11-2125-2011

Shay-El Y, Alpert P (1991) A diagnostic study of winter diabatic heating in the Mediterranean in relation to cyclone. Quart J Roy Meteor Soc 117:715–747

Shohami D, Dayan U, Morin E (2011) Warming and drying of the eastern Mediterranean: additional evidence from trend analysis. J Geophys Res Atmos 116:1–12

Sousa PM, Trigo RM, Aizpurua P, Nieto R, Gimeno L, Garcia-Herrera R (2011) Trends and extremes of drought indices throughout the 20th century in the Mediterranean. Nat Hazards Earth Syst Sci 11:33–51. https://doi.org/10.5194/nhess-11-33-2011

Takeshima A, Kim H, Shiogama H, Lierhammer L, Scinocca JF, Seland Ø, Mitchell D (2020) Global aridity changes due to differences in surface energy and water balance between 1.5°C and 2°C warming. Environ Res Lett 15:0940a7. https://doi.org/10.1088/1748-932

Toreti A, Xoplaki E, Maraun D, Kuglitsch FG, Wanner H, Luterbacher J (2010) Characterization of extreme winter precipitation in Mediterranean coastal sites and associated anomalous atmospheric circulation patterns. Nat Hazards Earth Syst Sci 10:1037–1050

Tzvetkov E, Assaf G (1982) The Mediterranean heat storage and Israeli precipitation. Water Res 18:1036–1040

Ulbrich U, Lionello P, Belušić D et al (2012) Climate and the Mediterranean: synoptic patterns, temperature, precipitation, winds and their extremes. In: Lionello P (ed) The climate of the Mediterranean region: from the past to the future. Elsevier, London, pp 301–346

Walsh RPD, Lawler DM (1981) Rainfall seasonality: description, spatial patterns and change through time. Weather 36:201–208

Ward JH (1963) Hierarchical grouping to optimize an objective function. J Am Stat Assoc 58(301):236–244

Winkler DE, Belnap J, Hoover D, Reed SC, Duniway MC (2019) Shrub persistence and increased grass mortality in response to drought in dryland systems. Glob Chang Biol 25(9):3121–3135

Xoplaki E, Gonzalez-Rouco JF, Luterbacher J, Wanner H (2004) Wet season Mediterranean precipitation variability: influence of large-scale dynamics and trends. Clim Dyn 23:63–78

Yosef Y, Saaroni H, Alpert P (2009) Trends in daily rainfall intensity over Israel 1950/1-2003/4. The Open Atmos Sci J 3:196–203

Yosef Y, Aguilar E, Alpert P (2019) Changes in extreme temperature and precipitation indices: using an innovative daily homogenized database in Israel. Int J Climatol 39(13):5022–5045

Ziv B (2001) A subtropical rainstorm associated with a tropical plume over Africa and the Middle East. Theor App Clim 69(1/2):91–102

Ziv B, Dayan U, Kushnir Y, Roth C, Enzel Y (2006) Regional and global atmospheric patterns governing rainfall in the southern Levant. Int J Climatol 26:55–73

Ziv B, Saaroni H, Pargament R, Harpaz T, Alpert P (2014) Trends in rainfall regime over Israel, 1975-2010, and their relationship to large-scale variability. Reg Environ Chang 14(5):1751–1764

Springer